

Delivery of GABA_ARs to Synapses Is Mediated by HAP1-KIF5 and Disrupted by Mutant Huntingtin

Alison E. Twelvetrees,¹ Eunice Y. Yuen,² I. Lorena Arancibia-Carcamo,¹ Andrew F. MacAskill,¹ Philippe Rostaing,³ Michael J. Lumb,¹ Sandrine Humbert,⁴ Antoine Triller,³ Frederic Saudou,⁴ Zhen Yan,² and Josef T. Kittler^{1,*}

¹Department of Neuroscience, Physiology, and Pharmacology, University College London, Gower Street, London, WC1E 6BT, UK

²Department of Physiology and Biophysics, State University of New York at Buffalo, Buffalo, NY 14214, USA

³INSERM U789, Biologie Cellulaire de la Synapse N&P, Ecole Normale Supérieure Paris, 46 Rue d'Ulm 75005 Paris, France

⁴Institut Curie, Unite Mixte de Recherche 146, Centre National de la Recherche Scientifique, Building 110, Centre Universitaire, 91405, Orsay Cedex, France

*Correspondence: j.kittler@ucl.ac.uk

DOI 10.1016/j.neuron.2009.12.007

SUMMARY

The density of GABA_A receptors (GABA_ARs) at synapses regulates brain excitability, and altered inhibition may contribute to Huntington's disease, which is caused by a polyglutamine repeat in the protein huntingtin. However, the machinery that delivers GABA_ARs to synapses is unknown. We demonstrate that GABA_ARs are trafficked to synapses by the kinesin family motor protein 5 (KIF5). We identify the adaptor linking the receptors to KIF5 as the huntingtin-associated protein 1 (HAP1). Disrupting the HAP1-KIF5 complex decreases synaptic GABA_AR number and reduces the amplitude of inhibitory post-synaptic currents. When huntingtin is mutated, as in Huntington's disease, GABA_AR transport and inhibitory synaptic currents are reduced. Thus, HAP1-KIF5-dependent GABA_AR trafficking is a fundamental mechanism controlling the strength of synaptic inhibition in the brain. Its disruption by mutant huntingtin may explain some of the defects in brain information processing occurring in Huntington's disease and provides a molecular target for therapeutic approaches.

INTRODUCTION

Synaptic inhibition plays a critical role in regulating neuronal excitability and information processing in the brain. The number of GABA_ARs expressed in the surface membrane and at synaptic sites is a critical determinant of inhibitory synapse strength (Arancibia-Carcamo and Kittler, 2009; Jacob et al., 2008), but the molecular machinery that deliver GABA_ARs to synapses remain unclear. Importantly, the role of kinesin family (KIF) microtubule motors in regulating the strength and plasticity of GABAergic transmission is unknown, as is the identity of the adaptor molecules which link GABA_ARs to their trafficking motors.

Alterations in protein trafficking to neuronal membranes, including altered trafficking of GABA_ARs, occur in a number of neurological and psychiatric diseases (Jacob et al., 2008; Olkko-nen and Ikonen, 2006). Altered GABA_AR trafficking may underlie

or exacerbate disease progression by altering the excitatory/inhibitory balance, leading to neuronal excitotoxicity and/or disrupted information processing (Arancibia-Carcamo and Kittler, 2009; Jacob et al., 2008). In Huntington's disease (HD), a polyglutamine expansion in the huntingtin protein (polyQ-htt) results in cell death and neurodegeneration of specific neuronal populations, leading to uncontrolled movements, personality changes, dementia, and eventually death within 10–20 years of the first symptoms. In addition to roles in regulating apoptosis and transcription, huntingtin may have a neurotoxic role in HD by altering intracellular transport of proteins, including transport of NMDA receptors (Fan and Raymond, 2007; Gunawardena et al., 2003; Smith et al., 2005; Szebenyi et al., 2003; Gauthier et al., 2004). Whether mutant huntingtin disrupts GABA_AR trafficking, leading to compromised inhibition and disruption of the excitatory/inhibitory balance, remains unknown.

A key mediator of pathological alterations in protein trafficking produced by polyQ-htt is the huntingtin-associated protein 1 (HAP1; (Gauthier et al., 2004; Li and Li, 2005; Li et al., 1995). HAP1 interacts directly with GABA_ARs and facilitates their recycling back to synapses after they have been internalized from the surface membrane, and so can regulate the strength of inhibitory synaptic transmission (Kittler et al., 2004), but how HAP1 regulates GABA_AR trafficking to synapses and whether this trafficking is a target for mutant polyQ-htt remains unknown.

Here, using biochemical, imaging, and electrophysiological approaches, we show that HAP1 is an adaptor that links GABA_ARs to KIF5 motors, forming a motor protein complex for rapid delivery of GABA_ARs to synapses. Furthermore, mutant huntingtin containing a polyQ expansion that disrupts HAP1 function (Gauthier et al., 2004; Li et al., 1995) inhibits this KIF5-dependent GABA_AR trafficking and synaptic delivery. Thus, KIF5-dependent transport is critical for delivery of GABA_ARs to inhibitory synapses, and disruption of this complex by mutant huntingtin may lead to altered synaptic inhibition and increased neuronal excitability in Huntington's disease.

RESULTS

The Delivery of GABA_ARs to Synapses Is Mediated by the Motor KIF5

The kinesin motor protein KIF5 is a critical determinant of intracellular transport processes in neurons (Hirokawa and

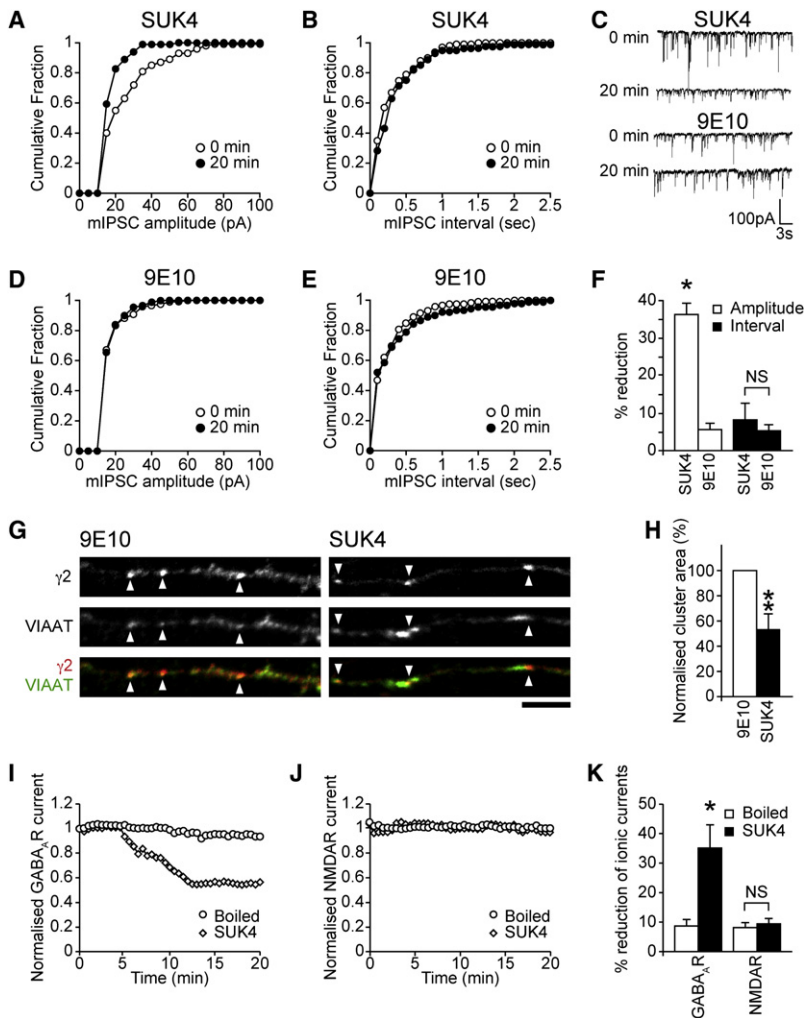


Figure 1. KIF5 Delivers GABA_ARs to Synapses

(A–F) mIPSCs in neurons dialyzed with either SUK4 or control 9E10 antibodies. Cumulative distribution plots show mIPSC amplitudes shifted leftward in SUK4-dialyzed (A) but not control 9E10 dialyzed (D) neurons at $t = 20$ compared with $t = 0$ min. There is no change in mIPSC interval for either SUK4 or 9E10 (B and E). Representative traces reveal time-dependent reduction in mIPSC sizes upon dialysis of SUK4, but not control 9E10 antibody (C). Summary bar graphs (F) show the percentage (mean and standard error of the mean [\pm SEM]) reduction of mIPSC amplitude and interval produced by SUK4 or 9E10 after 20 min of antibody dialysis (SUK4, $n = 7$; 9E10, $n = 5$; $*p < 0.05$).

(G and H) Immunofluorescence and CLSM reveals that SUK4 treatment of neurons reduces synaptic GABA_AR cluster area (arrowheads) compared with 9E10 control (scale bar = 5 μ m). Error bars, SEM; $n = 3$ experiments, 15 neurons; $**p < 0.01$ (Student's t test).

(I–K) Evoked whole-cell recordings of GABA_AR currents (I) and NMDAR currents (J) were recorded from neurons dialyzed with either the SUK4 or boiled (inactive) antibody control. SUK4 antibody caused a gradual reduction of GABA_AR currents, but the boiled antibody control had no effect. Dialysis of either antibody failed to effect NMDAR currents. (K) Summary bar graph showing the percentage reduction in ionic currents. Error bars, SEM; $n = 6$ –7; $*p < 0.05$.

KIF5 does not selectively transport GABA_ARs with particular kinetics (see Table S1 available online). Similar results were also seen with SUK4 and 9E10 Fab fragments (Figures S1A–S1E). Thus, our results support a key role for KIF5 function in maintaining inhibitory synaptic transmission.

We hypothesized that the effect of SUK4 on inhibitory transmission was mediated by blocking KIF5-dependent GABA_AR delivery to synapses. To test this, SUK4 or control 9E10 antibody was introduced into cultured neurons by complexing with a membrane permeant carrier peptide (Coulpier et al., 2002; Morris et al., 2001) and the effect on surface GABA_AR cluster area was determined using immunofluorescence and confocal laser scanning microscopy (CLSM). Cell surface synaptic GABA_AR clusters were identified with an antibody to the extracellular domain of the GABA_AR $\gamma 2$ subunit, while antibodies to the vesicular inhibitory amino acid transporter (VIAAT; a marker of inhibitory presynaptic terminals [Dumoulin et al., 1999]) were used to identify inhibitory synapses on neuronal dendrites. A mouse secondary antibody verified that SUK4 penetrated the neurons (Figure S1G). Neurons treated with SUK4 showed a significant decrease in GABA_AR cluster area in dendrites compared with control mock-treated or 9E10 treated neurons (Figures 1G and 1H; SUK4 treatment reduced GABA_AR cluster area by $46.5\% \pm 11.9\%$ compared with 9E10 controls, $n = 5$, $p < 0.01$), but with no change in the ratio of synaptic to non-synaptic GABA_AR clusters (Figure S1F), strongly suggesting that blocking KIF5 activity decreases the delivery of GABA_ARs to synapses.

Takemura, 2005). To investigate if KIF5 activity is important for inhibitory transmission, we carried out whole-cell patch-clamp recordings to measure inhibitory synaptic transmission in cortical neurons dialyzed via the electrophysiological recording pipette with an antibody demonstrated to block KIF5 motor protein activity (kinesin function blocking antibody SUK4 [Ingold et al., 1988; Jaulin et al., 2007]), which does not inhibit myosin- or dynein-based motility (Bi et al., 1997; Lane and Allan, 1999). This was compared with neurons dialyzed with a control antibody (9E10) that does not recognize KIF5. Dialysis of SUK4 (Figures 1A, 1C, and 1F) caused a rapid reduction in mIPSC amplitude within 20 min of recording (Figure 1F: SUK4, $36.2\% \pm 3\%$ reduction in mean mIPSC amplitude $n = 7$, $p < 0.05$), as can clearly be seen in representative mIPSC traces (Figure 1C) and by a leftward shift to smaller amplitudes in cumulative probability plots (Figure 1A). In contrast there was no significant decrease in mean mIPSC amplitude in control 9E10 dialyzed neurons (Figures 1D and 1F: 9E10, $5.6\% \pm 1.7\%$ reduction, $n = 5$). Neither SUK4 nor 9E10 antibody was found to affect mIPSC interval (Figures 1B, 1E, and 1F: SUK4, $8.2\% \pm 4.4\%$ reduction in mean mIPSC interval; 9E10, $5.3\% \pm 1.6\%$ reduction). Dialysis of SUK4 antibody did not affect mIPSC kinetics, implying that

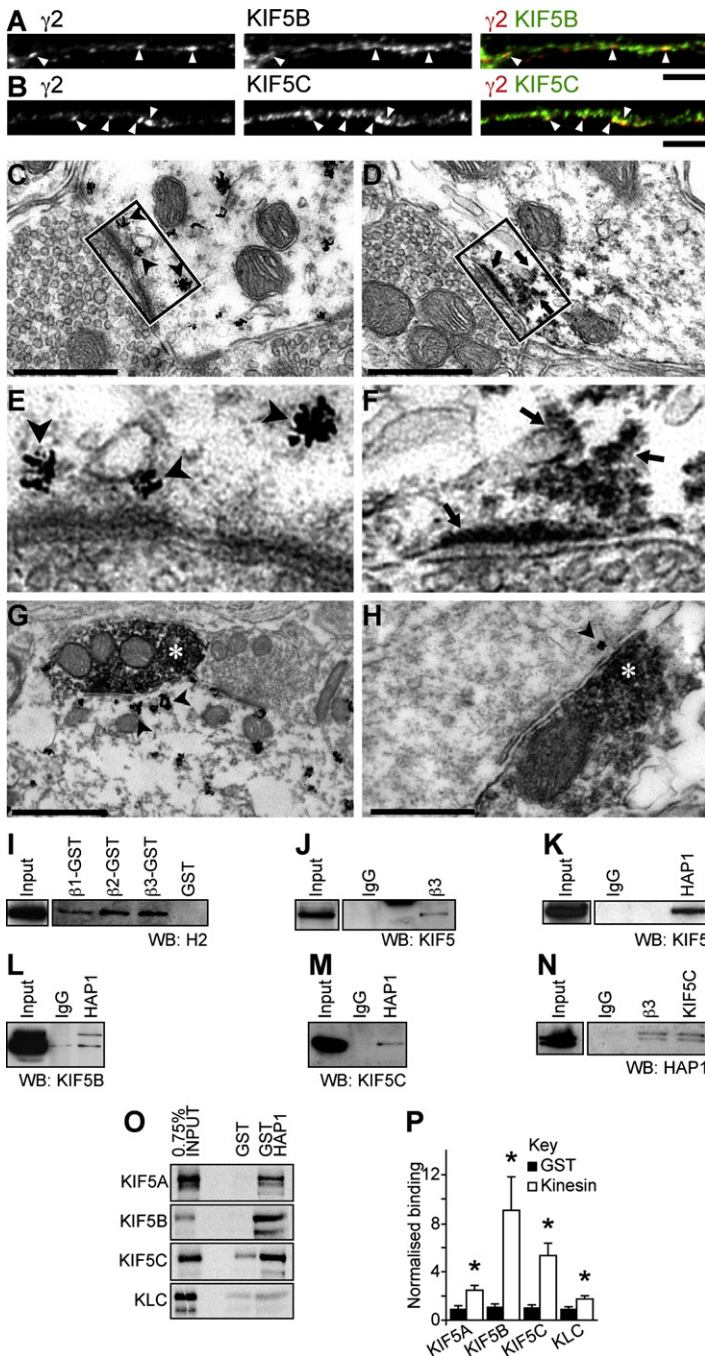


Figure 2. Endogenous HAP1/KIF5/GABA_A Complexes

(A–H) KIF5 colocalizes with GABA_ARs and is found at inhibitory post-synapses. (A and B) Neurons costained with antibodies to the GABA_AR γ 2 subunit (red) and either anti-KIF5B (A) or anti-KIF5C (B) (green; scale bar = 5 μ m). Both KIF5B and KIF5C are found to colocalize (yellow) with a subset of γ 2 containing GABA_AR clusters in dendrites (arrowheads). (C–H) Ultrastructural localization of KIF5 heavy chains (scale bars, C, D, and H = 0.5 μ m; G = 1 μ m). Discontinuous deposits of gold-toned silver-intensified nanogold particles immunolabeling KIF5 (C, E, G, and H arrowheads) or electron-dense HRP reaction product (D and F, arrows) are frequently seen close to the postsynaptic membrane opposed to presynaptic boutons containing pleomorphic populations of vesicles indicative of inhibitory synapses (C, D, E, and F) or GAD HRP immunolabeled boutons (G and H, white star, from spinal cord and hippocampal tissue, respectively). (D) KIF5C localized at the inhibitory postsynaptic membrane. (E) Boxed region in (C). (F) Boxed region in (D). (E and F) KIF5 is frequently seen associated with vesicles close to the postsynaptic membrane.

(I–N) Coprecipitation and pull-down assays of GABA_ARs, KIF5 and HAP1 from rat brain tissue reveals they form complexes in vivo (WB = western blot; input = 5%–15% of the brain lysate present in the assay; each blot represents at least three repetitions). Western blots of pull downs with GST fusion proteins of the intracellular loops of GABA_AR subunits β 1, 2, and 3 show they were able to bring down kinesin heavy chains (I) as was immunoprecipitation with antibodies against the β 3 subunits of GABA_ARs (J). HAP1 antibodies also immunoprecipitate KIF5 when western blots are probed with a pan KIF5 antibody (K) or with specific antibodies against both KIF5B (L) and KIF5C (M). In reverse immunoprecipitation experiments with anti-GABA_AR β 3 antibodies and anti-KIF5C, HAP1a and HAP1b are present in immune pellets (N).

(O and P) The kinesin motor subunits KIF5A–C and kinesin light chain (KLC) were translated in vitro and labeled with [³⁵S]-methionine. The resulting protein was subjected to pull-down assay with GST-HAP1, and GST alone as control, separated by SDS-PAGE (O) and radioactivity detected using a phosphor storage screen. (P) Summary bar graph of relative binding of KIF5 subunits to HAP1. Error bars, SEM; n = 5; *p < 0.05, Student's t test.

whereas neither active nor inactive SUK4 affected NMDAR-mediated responses (Figures 1J and 1K: SUK4: 9.4% \pm 1.8% reduction in NMDA response, n = 7; boiled SUK4: 8.1% \pm 1.7%, n = 7), further supporting the specificity of KIF5 for selectively trafficking GABA_ARs to synapses.

HAP1 Is the Adaptor Linking KIF5 to GABA_ARs

If KIF5 is important for synaptic delivery of GABA_ARs, then we would expect to detect localization of KIF5 and GABA_ARs to the same neuronal compartments. In agreement with this, immunofluorescence and CLSM with

We also compared the effect of blocking KIF5 activity on GABA_AR responses with its effect on NMDA receptor (NMDAR) mediated responses, which are trafficked by a different KIF, the motor protein KIF17 (Guillaud et al., 2003; Setou et al., 2000). Compared with control inactive (boiled) SUK4 antibody (Figures 1I and 1K), SUK4 dialysis rapidly and dramatically reduced GABA_AR mediated whole-cell responses in recorded neurons (Figures 1I and 1K: 35.1% \pm 7.9% reduction in GABA response within 20 min with SUK4, n = 6, p < 0.05, compared with 8.7% \pm 2.2% reduction for inactive boiled SUK4, n = 7),

antibodies to the GABA_AR γ 2 subunit and antibodies specific to KIF5B (Figure 2A) or KIF5C (Figure 2B), revealed that a proportion of KIF5 staining colocalized with GABA_AR clusters in the neuronal somata and dendrites of cultured hippocampal and cortical neurons (see also Figure S2 for whole images of hippocampal neurons and for labeling of cortical neurons). Furthermore, electron microscopy of in vivo hippocampus and rat ventral spinal cord, revealed that KIF5-positive deposits were consistently found in the vicinity of postsynaptic membranes and decorating the postsynaptic side of symmetrical type 2

contacts, defined as inhibitory by the pleomorphic nature of the vesicles within the presynaptic boutons and by their narrow (15–20 nm) synaptic cleft (Figures 2C–2H). With pre-embedding immunolabeling and gold-toned silver intensified nanogold particles, KIF5 staining was found associated with small subsynaptic intracellular cisternae, which were often located below or at the edge of postsynaptic differentiations that may be part of subsynaptic tubulovesicular endosomes (Figures 2C and 2E). Double detection of GAD and KIF5, with immunoperoxidase and gold-toned silver-intensified nanoparticles, respectively, confirmed the inhibitory nature of the presynaptic terminals (Figures 2G and 2H).

We would also expect to detect protein complexes of KIF5 and GABA_ARs in vivo. To investigate this we carried out glutathione-S-transferase (GST) pull downs and coimmunoprecipitation assays from rat brain lysate. GST-fusion proteins of the GABA_AR β 1-3 subunit intracellular domains (Figure 2I), or rat brain immunoprecipitated GABA_ARs (Figure 2J) could readily coprecipitate KIF5 heavy chains, providing evidence that KIF5 motor proteins form complexes with GABA_ARs in vivo. Motor proteins often determine cargo selectivity by linking to the cargo via an adaptor protein (Hirokawa and Takemura, 2005). HAP1 is involved in motor-protein-dependent transport of neuronal cargo, associating with motor protein complexes (Engelender et al., 1997; Gauthier et al., 2004; Li et al., 1998; McGuire et al., 2006), as well as interacting directly with GABA_ARs (Kittler et al., 2004), and therefore was a good candidate adaptor to link GABA_AR transport vesicles with KIF5 motors. HAP1 immunoprecipitated from solubilized brain extracts readily coprecipitated KIF5, as demonstrated with either a pan anti-KIF5 antibody (which recognizes all three KIF5 heavy chains, Figure 2K) or using anti-KIF5B and anti-KIF5C-specific antibodies (Figures 2L and 2M, respectively). In the reverse experiment, HAP1 readily coprecipitated with immunoprecipitated KIF5C or GABA_AR β 3 subunits, further confirming that in vivo GABA_ARs are found in complexes with HAP1 and KIF5 (Figure 2N). To test if the interaction between HAP1 and KIF5A-C heavy chains was direct, we performed GST fusion protein affinity purification experiments with GST-HAP1 and individual ³⁵S-methionine-labeled KIF5A-C heavy chains or the kinesin light chain (KLC), which confirmed a direct interaction of KIF5 heavy chains with HAP1 (highest for KIF5B and KIF5C isoforms; Figures 2O and 2P). Thus HAP1 is the adaptor linking KIF5 to GABA_ARs.

KIF5 Mediates Insertion of GABA_ARs into the Surface Membrane at Synapses

To further investigate the mechanism of KIF5-dependent GABA_AR trafficking we identified the molecular determinants of the HAP1-KIF5 interaction. KIF5 heavy chains comprise an N-terminal motor domain and a C-terminal nonmotor domain. Initial experiments, using coimmunoprecipitation and coexpression of epitope tagged KIF5C N-terminal motor domain or C-terminal nonmotor domain proteins, revealed that HAP1 interacts with the KIF5C nonmotor domain (Figure S3), which comprises the stalk domain, the kinesin light chain binding domain, and the cargo binding domain. Using additional GFP tagged constructs for KIF5B (or KIF5C; not shown), lacking either the stalk domain or both the stalk and light chain binding regions,

we determined that the C-terminal cargo binding domain of KIF5 is the minimal region sufficient for mediating an interaction with HAP1, as shown by the fact that GST-HAP1 (Figure S3D) or GST-HAP1 fragments (Figures 3A–3C) could readily pull down the C-terminal domain of KIF5B (residues 814–963, from here on called the HAP1-binding domain, or HBD; see Figure 3A). In complementary GST pull-down experiments with GST-HAP1 deletion constructs (Figures 3A–3C), we also determined that a region containing coiled-coil domains 1 and 2 (part of the HAP N-terminal homology domain) was sufficient for interacting with the C-terminal region of the KIF5 motor (Figures 3B and 3C).

We used the HAP1 binding domain of KIF5 (KIF5-HBD) as a dominant negative construct to further investigate the consequences of disrupting KIF5-dependent GABA_AR trafficking to synapses. Using surface biotinylation to quantify surface GABA_AR levels, we found that, compared with control GFP-transfected neurons, neurons expressing the ^{GFP}KIF5B-HBD produced a significant decrease in the cell surface number of GABA_ARs containing β 3 subunits ($68.5\% \pm 6.0\%$ of control, $n = 8$, $p < 0.005$, Figures 3D–3F), whereas surface levels of either the transferrin receptor (TfR) or the NMDAR were unaffected (Figures S3E and S3F). The source of GABA_ARs from the internal pool that supplies fast synaptic receptor insertion remains unknown. However, GABA_ARs have been previously demonstrated to be rapidly reinserted into the membrane from an intracellular pool of internalized receptors (Kittler et al., 2004). After labeling this intracellular pool of GABA_ARs with biotin, the loss of biotinylated internal GABA_ARs after a second biotin cleavage (see Experimental Procedures) provides a measure of receptor insertion rate into the membrane (Ehlers, 2000; Kittler et al., 2004). Internal biotinylated GABA_ARs remaining during the time course were then compared with those at the start of the reinsertion time course (i.e., time 0 in Figure 3G), designated as 100%. We found that expressing ^{GFP}KIF5B-HBD in neurons resulted in a significant reduction in the loss of the internal biotinylated receptor pool (i.e., more internal biotinylated receptors remained) compared with GFP controls. This gives a significant decrease in GABA_AR insertion levels at 30 and 60 min upon disruption of HAP1/KIF5-dependent trafficking (Figures 3G and 3H: at 30 min $38.6\% \pm 2.4\%$ receptors remained in the internal pool for ^{GFP}KIF5B-HBD transfected neurons compared with $27.1\% \pm 3.9\%$ receptors remaining in the internal pool for GFP control transfected neurons; at 60 min $25.1\% \pm 2.1\%$ for ^{GFP}KIF5B-HBD compared with $14.2\% \pm 2.9\%$ for GFP control; $n = 5$, $p < 0.05$). In contrast GABA_AR endocytosis was not affected by expressing ^{GFP}KIF5B-HBD (Figures S3G, S3H). Our results demonstrate that disrupting KIF5-dependent trafficking by expressing ^{GFP}KIF5B-HBD decreases receptor insertion into the surface membrane.

Functional confirmation that this decrease in trafficking resulted in a loss of synaptic receptors was observed from whole-cell patch-clamp recordings (Figures 4A–4E). Neurons transfected with ^{GFP}KIF5B-HBD showed a significant decrease in mIPSC amplitudes compared with GFP-transfected neurons, (Figures 4A, 4C, and 4D; mean mIPSC amplitude in ^{GFP}KIF5B-HBD transfected neurons 17.8 ± 2.4 pA, $n = 6$, compared with 27.8 ± 3.7 pA, $n = 5$, for control GFP transfected neurons, $p < 0.05$), which was also indicated by a leftward shift toward

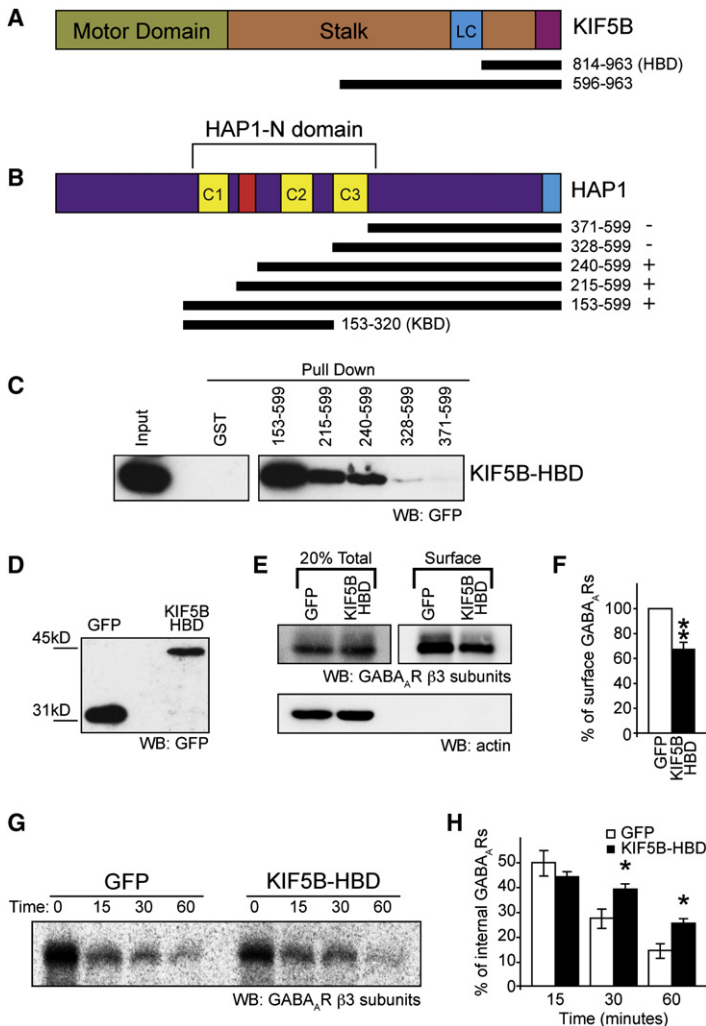


Figure 3. A HAP1-KIF5 Complex Mediates Reinsertion of GABA_ARs from the Intracellular Pool into the Surface Membrane

(A–C) Identification of the binding sites on HAP1 and KIF5. (A and B) Schematic diagrams of KIF5 and HAP1 constructs relative to the full-length proteins. (C) ^{GFP}KIF5B residues 814–963 (designated KIF5B-HAP1 Binding Domain: KIF5B-HBD) is sufficient for binding to a central region of HAP1 (residues 153–328) in a pull-down assay. (D) GFP and ^{GFP}KIF5B-HBD expression in lysate from transfected neurons used for biotinylation assays (E–H) detected by western blotting (WB) with GFP antibodies.

(E and F) Expression of KIF5B-HBD reduces surface expression of GABA_ARs in neurons as revealed by surface biotinylation and western blotting with anti-GABA_Aβ3 subunit antibodies. Surface receptors were labeled with biotin and surface expression normalized to the total number of receptors in the system. Actin blot (lower panel, E) shows actin present in total lysate (the saved 20% fraction) of cells, but exclusion from the surface only biotinylated fraction. (F) Summary bar graph shows surface expression normalized to GFP control (n = 8 experiments; error bars, SEM; **p < 0.005, Student's t test).

(G and H) Expression of KIF5B-HBD reduces reinsertion of internalized GABA_ARs. (G) A representative western blot of the reinsertion time course, bands represent the protected internal pool of GABA_ARs following 0, 15, 30, and 60 min of reinsertion. The loss of biotinylated GABA_ARs provides a measure of receptor reinsertion. (H) Expression of ^{GFP}KIF5B-HBD causes a reduced rate of reinsertion shown by increased levels of internal receptors at 30 and 60 min time points (n = 5; error bars, SEM; *p < 0.05, Student's t test).

lower amplitudes in the cumulative distribution plots (Figure 4A). An even greater reduction was seen upon neuronal expression of ^{GFP}KIF5C-HBD (Figures S4A and S4D; ^{GFP}KIF5C-HBD: 12.7 ± 1.2 pA, n = 8, compared with GFP: 27.4 ± 2.0 pA, n = 6, p < 0.05; equivalent to a 53.6% ± 4.4% reduction in mean amplitude for ^{GFP}KIF5C-HBD, compared with the 36.0% ± 8.6% reduction seen for ^{GFP}KIF5B-HBD). In contrast ^{GFP}KIF5B-HBD or ^{GFP}KIF5C-HBD expression caused no significant alteration in mIPSC interval (Figures 4B, 4E, S4B, and S4E; mIPSC average interval GFP: 0.21 ± 0.02 s, n = 5, ^{GFP}KIF5B-HBD: 0.22 ± 0.01 s, n = 6; GFP: 0.20 ± 0.02 s, n = 6, ^{GFP}KIF5C-HBD: 0.24 ± 0.01 s, n = 8). Further supporting the idea that HAP1-KIF5-dependent reinsertion of GABA_ARs plays a critical role in delivery of GABA_ARs to synapses, we also found that expression of KIF5-HBD decreased the size of GABA_AR clusters, as demonstrated by immunofluorescence and CLSM (GABA_AR cluster area in KIF5B-HBD expressing neurons was 72.9% ± 10.3% of control GFP expressing neurons, n = 5, p < 0.01, see Figures 4F and 4G) without producing a change in the ratio of the number of synaptic to the number of nonsynaptic GABA_AR clusters (Figure S4F).

To further support the role of the HAP1/KIF5 complex for trafficking GABA_ARs to synapses, we also investigated the functional consequences of expressing in neurons the domain on HAP1 to which KIF5 binds (i.e., the HAP1-KIF5 binding domain; HAP1-KBD; Figure 3B). Compared with neurons expressing GFP, neurons expressing ^{GFP}HAP1-KBD showed reduced mIPSC amplitudes, (Figures 4H, 4J, and 4K; mIPSC amplitude in GFP-expressing neurons: 37.1 ± 2.4 pA, n = 8, and 22.9 ± 2.1 pA in ^{GFP}HAP1-KBD-expressing neurons, n = 7, p < 0.01), while similar to expression of KIF5-HBD, mIPSC frequency remained unaffected (Figures 4I, 4J, and 4L; GFP: 5.1 ± 0.7 Hz, n = 8; HAP1-KBD: 4.4 ± 0.4 Hz, n = 7). In contrast to the effects observed on GABA_AR mIPSC amplitude upon expression of KIF5-HBD or HAP1-KBD, targeting the function of the NMDAR motor KIF17, which does not interact with HAP1 (Figure S4L) and which blocks trafficking of NMDARs (Guillaud et al., 2003), had no effect on inhibitory synaptic function (Figures S4G–S4K). These results further support a critical role for the HAP1/KIF5 complex in trafficking GABA_ARs to synapses.

Our results suggest that HAP1 is a specificity adaptor for the recruitment of GABA_AR containing transport vesicles to a KIF5 transport pathway for their rapid delivery to synapses. To further validate the role of the HAP1-KIF5 complex, we used RNA interference (RNAi) to knock down HAP1 expression (Figures 5A–5C) and determined the effect on trafficking and synaptic inhibition. Similar to the effect of disrupting KIF5 function (by expressing KIF5-HBD), biotinylation experiments revealed that knocking down HAP1 (Figures 5A–5C) resulted in a substantial decrease in the number of surface GABA_ARs

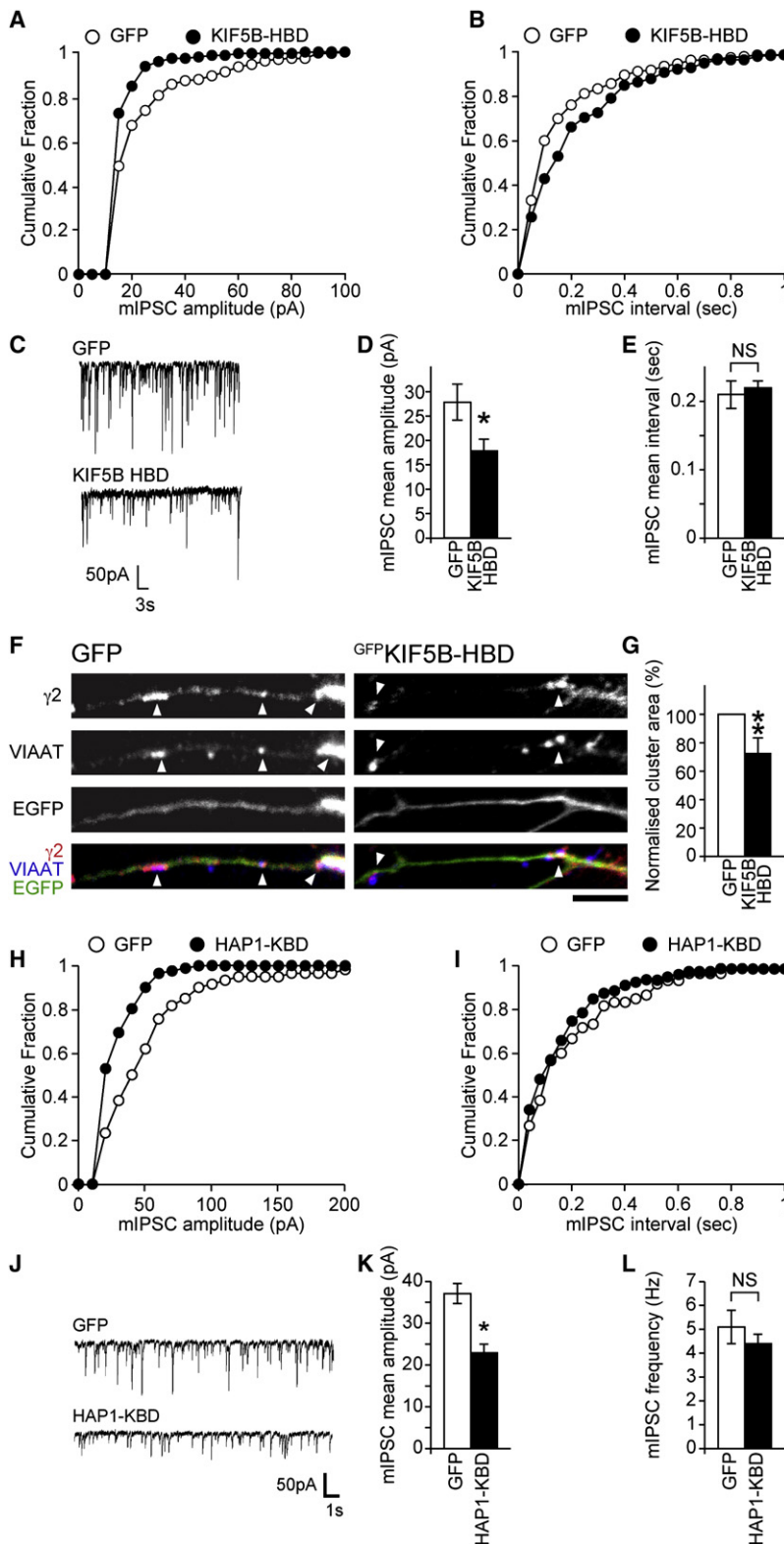


Figure 4. A HAP1-KIF5 Complex Can Modulate Inhibitory Synaptic Transmission

(A–E) Whole-cell recordings of mIPSCs from neurons transfected with ^{GFP}KIF5B-HBD or GFP control. (C) Representative traces demonstrating reduction in mIPSC amplitudes in cells transfected with ^{GFP}KIF5B-HBD compared with GFP-transfected cells. Cumulative distribution plots show the mIPSC amplitude shifts to smaller amplitudes in neurons transfected with ^{GFP}KIF5B-HBD (A), while there is no change in mIPSC interval (B). Summary bar graphs (D and E) show the average (mean \pm SEM) mIPSC amplitude and interval of transfected neurons (GFP, n = 5; KIF5B-HBD, n = 6; *p < 0.05). (F and G) GABA_AR cluster analysis reveals that neurons expressing ^{GFP}KIF5B-HBD show reduction in synaptic γ 2 clusters (arrowheads) compared with GFP control expressing cells (scale bar = 5 μ m). Error bars, SEM; n = 5 experiments, 26–27 neurons; **p < 0.01, (Student's t test).

(H–L) Whole-cell recordings of mIPSCs from neurons transfected with ^{GFP}HAP1-KBD or GFP control. (J) Representative traces demonstrating reduction in mIPSC amplitude in cells transfected with ^{GFP}HAP1-KBD compared with GFP-transfected cells. Cumulative distribution plots show the mIPSC amplitude shifts to smaller amplitudes in neurons transfected with ^{GFP}HAP1-KBD (H), while there is no change in mIPSC interval (I). Summary bar graphs (K and L) show the average (mean \pm SEM) mIPSC amplitude and frequency of transfected neurons (GFP, n = 8; HAP1-KBD, n = 7; *p < 0.05).

levels of TfR or the NMDAR (Figures S5A and S5B). Biotinylation experiments also revealed that HAP1 knockdown resulted in a significant reduction in rates of GABA_AR insertion into the membrane at 30 and 60 min compared with RNAi control transfected cells (Figures 5F and 5G). At 30 min the control RNAi cells had 25.3% \pm 2.6% of receptors remaining in the internal pool compared with 40.7% \pm 5.5% receptors remaining for HAP1 RNAi, while at 60 min the control RNAi cells had 13.0% \pm 2.2% receptors remaining in the internal pool compared with 25.2% \pm 5.6% in HAP1 RNAi-expressing cells; n = 7–9; p < 0.05), but HAP1 RNAi did not alter GABA_AR endocytosis (Figures S5C and S5D). In agreement with these observations, patch-clamp recordings of neurons expressing the HAP1 RNAi revealed that mIPSC amplitude, but not frequency, in neurons was dramatically reduced compared with the scrambled control RNAi (Figures 6A–6E: HAP1 RNAi mIPSC amplitude, 23.7 \pm 2.1 pA, n = 8 compared with control RNAi mIPSC amplitude 41.6 \pm 2.3 pA, n = 7, p < 0.05; HAP1 RNAi mIPSC frequency, 4.2 \pm 0.17 Hz, n = 8 compared with control RNAi mIPSC frequency

(for HAP1 RNAi-expressing neurons surface levels were 43.1% \pm 8.2% of control scrambled RNAi expressing neurons, n = 6, p < 0.0005, Figures 5D and 5E) without affecting the surface

4.2 \pm 0.25 Hz, n = 7). This correlates with the reduced size of synaptic GABA_AR clusters as determined by immunofluorescence and confocal imaging (70.4% \pm 8.3% of control, n = 3,

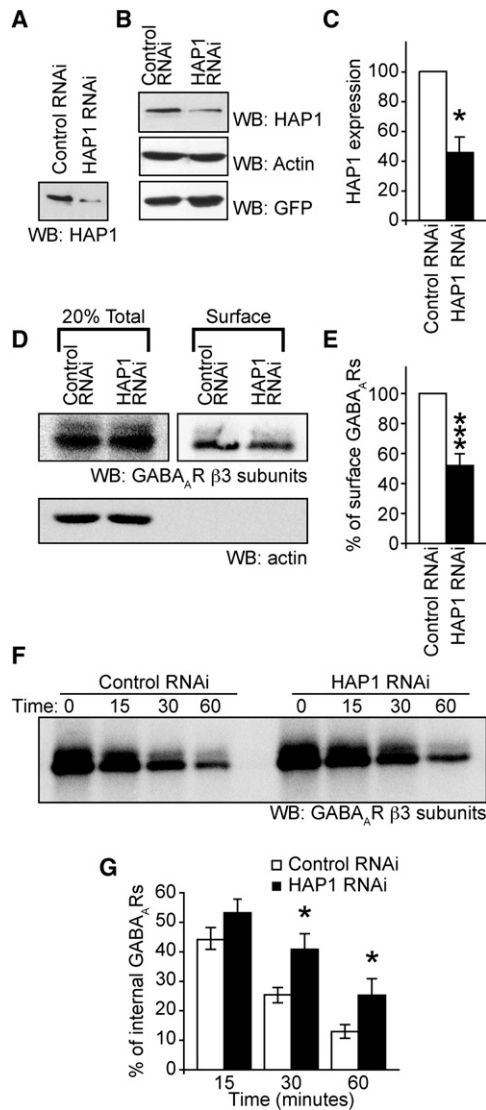


Figure 5. HAP1 Knockdown Disrupts Surface Targeting of GABA_ARs

(A–C) Western blots showing knockdown with HAP1 RNAi compared with a scrambled control RNAi of exogenous HAP1 expressed in HEK cells (A) or endogenous HAP1 in neurons (B). (C) Summary bar graph of knock down in neurons with HAP1 expression normalized to actin. Error bars, SEM; $n = 3$; $p < 0.05$, Student's *t* test.

(D and E) Expression of HAP1 RNAi reduces surface expression of GABA_ARs in neurons as revealed by surface biotinylation and western blotting with anti-GABA_AR- $\beta 3$ subunit antibodies ($n = 6$ experiments; error bars, SEM; *** $p < 0.0005$, Student's *t* test). Actin blot (D, lower panel) shows actin present in total lysate of cells, but exclusion from the surface only purified fraction of protein.

(F and G) Expression of HAP1 RNAi reduces reinsertion of internalized GABA_ARs. ($n = 9$; error bars, SEM; * $p < 0.05$, Student's *t* test). (F) A representative western blot of the reinsertion time course. (G) Expression of HAP1 RNAi causes a reduced rate of reinsertion shown by increased levels of internal receptors at 30 and 60 min time points. Error bars, SEM; $n = 7$ – 9 ; * $p < 0.05$, Student's *t* test.

$p < 0.05$, see Figures 6F and 6G), while no effect on the synaptic to nonsynaptic ratio of GABA_AR cluster numbers was observed (Figure S6A).

To further study the role of HAP1-dependent GABA_AR trafficking, we also performed live cell imaging experiments in neurons expressing GFP-labeled GABA_AR transport vesicles. We designed a new HAP1 (or control) shRNAi vector coexpressing GFP tagged $\gamma 2$ GABA_AR subunits ($\gamma 2^{\text{GFP}}$) such that neurons expressing GFP labeled GABA_ARs would also express either HAP1 RNAi or control RNAi (Figures S6B–S6E). By imaging over time, motile $\gamma 2^{\text{GFP}}$ labeled GABA_AR transport vesicles in dendrites were visualized using kymographs (Figures 6I–6J) that were created by projecting sequential line scans through a process of interest onto the *y* axis (Macaskill et al., 2009). Stationary GABA_ARs are seen as straight lines and moving GABA_AR vesicles as diagonal lines. Using this technique, $\gamma 2^{\text{GFP}}$ -GABA_ARs could be seen to be present in both moving and stationary clusters in dendrites. We investigated the effect of altering HAP1 expression levels on the dynamics of $\gamma 2^{\text{GFP}}$ -GABA_AR vesicle movement in neurons coexpressing HAP1 shRNAi to reduce HAP1 expression levels (Figures 6I and 6K). Compared with control neurons (Figures 6I and 6I'), far fewer GABA_AR vesicles could be observed to be moving, assessed over a 5 min period (Figures 6J and 6J'), most easily seen in the masked kymographs (bottom panels of Figures 6I' and 6J') which show only the tracks of moving vesicles. HAP1 knockdown also significantly affected GABA_AR vesicle run length with $\gamma 2^{\text{GFP}}$ -GABA_AR vesicles moving far shorter distances in the HAP1 RNAi-expressing neurons than in control cells (Figure 6H; average track run length in control RNAi cells $32.9 \pm 3.1 \mu\text{m}$, and in HAP1 RNAi cells $23.6 \pm 2.9 \mu\text{m}$, $p < 0.05$, $n = 45$ tracks in each case).

Mutant PolyQ Huntingtin Disrupts GABA_AR Trafficking, Synaptic Receptor Delivery, and Inhibitory Transmission

HAP1 function is disrupted by the mutant (polyQ) version of huntingtin that causes Huntington's disease (Gauthier et al., 2004; Li et al., 1995). HAP1-KIF5-dependent GABA_AR trafficking is therefore a likely target for disruption in HD, which would lead to pathological alterations in inhibition. To further investigate this possibility, we performed live cell imaging experiments in neuronal cells derived from knock-in mice, where a CAG expansion (encoding poly-glutamines) has been inserted into the endogenous mouse *htt* gene (Trettel et al., 2000). These cell lines reflect the closest situation to HD patients, because wild-type or polyQ-*htt* is expressed at endogenous levels. Neuronal cells containing either two copies of wild-type *htt* (wild-type neuronal cells, +/+), or two copies of mutant *htt* (homozygous mutant neuronal cells, 109Q/109Q) were transfected with GFP tagged GABA_ARs ($\alpha 1\beta 3\gamma 2^{\text{GFP}}$) and imaged using live cell video microscopy to monitor the trafficking dynamics of $\text{GFP}^{\text{GABA}_A\text{R}}$ transport vesicles (Figures 7A–7C and Movies S1 and S2). By tracking $\text{GFP}^{\text{GABA}_A\text{R}}$ transport vesicles, the influence of wild-type (WT) or polyQ-*htt* on vesicle velocity and vesicle run length was determined. These experiments revealed a significant decrease in the velocity (Figures 7A and 7C, 109Q/109Q cells, $0.36 \pm 0.01 \mu\text{m/s}$ compared with +/+ controls, $0.41 \pm 0.01 \mu\text{m/s}$, $p < 0.05$) and run length (Figures 7B and 7C, 109Q/109Q cells, $5.4 \pm 0.6 \mu\text{m}$ compared with +/+ cells, $7.6 \pm 0.6 \mu\text{m}$, $p < 0.05$) of

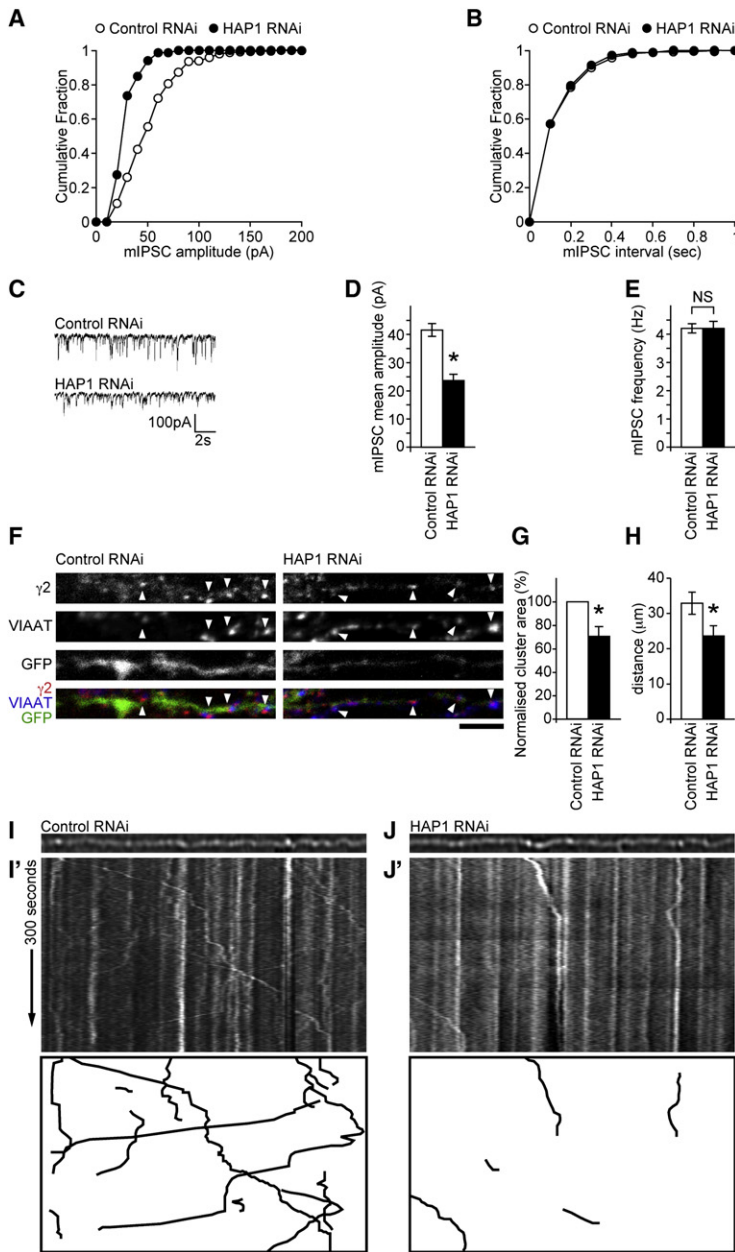


Figure 6. HAP1 Knockdown Disrupts Synaptic Targeting and Trafficking of GABA_ARs

(A–E) Whole-cell recordings of mIPSCs from neurons transfected with HAP1 RNAi or scrambled RNAi control. (C) Representative traces demonstrating reduction in mIPSC sizes in cells transfected with HAP1 RNAi, compared with scrambled control transfected cells. Cumulative distribution plots show the mIPSC amplitude shifts to smaller amplitudes in neurons transfected with HAP1 RNAi (A), while there is no change in mIPSC interval (B). Summary bar graphs (D and E) show the average (mean ± SEM) mIPSC amplitude and frequency of transfected neurons (control RNAi, n = 7; HAP1 RNAi, n = 8; *p < 0.05).

(F and G) GABA_AR cluster analysis reveals that neurons expressing HAP1 RNAi show reduction in synaptic γ 2 clusters (arrowheads) compared with scrambled control expressing cells (scale bar = 5 μ m). Error bars, SEM; n = 3 experiments, 24–25 neurons; *p < 0.05 (Student's t test).

(I–J) The trafficking of γ 2^{GFP}-GABA_AR vesicles in neurons coexpressing either control RNAi or HAP1 RNAi were analyzed by video microscopy. (H) Distance traveled ± SEM (μ m) by γ 2^{GFP}-GABA_AR vesicles was reduced in neurons expressing the HAP1 RNAi compared with controls (n = 45 tracks each over four independent experiments and 9–14 cells; *p < 0.05, Student's t test). (I–J) Static images and kymographs showing GABA_AR vesicle movement through dendrites transfected with ^{GFP}GABA_ARs and either control (I and I') or HAP1 RNAi (J and J'). Bottom panels show masks of kymographs to allow visualization of only the moving vesicles.

^{GFP}GABA_AR transport vesicles in 109Q/109Q cells compared with control +/+ cells. The effects of polyQ-htt on ^{GFP}GABA_AR transport vesicle dynamics were occluded by coexpression of KIF5-HBD, which reduced GABA_AR vesicle trafficking to the same level in both +/+ and 109Q/109Q cells (Figure S7). Our results strongly suggest that mutant polyQ-htt causes decreased accumulation of GABA_ARs at inhibitory synapses (leading to compromised inhibition) by reducing the processivity (Gauthier et al., 2004) and trafficking ability of HAP1-KIF5-dependent GABA_AR transport vesicles for receptor delivery to inhibitory synapses.

To address the functional consequences of altered HAP1-KIF5-dependent GABA_AR trafficking by polyQ-htt on inhibitory

synaptic transmission, we transfected cortical neurons with ^{GFP}WT-htt or ^{GFP}polyQ-htt constructs and used electrophysiology to look at mIPSC properties. Compared with ^{GFP}WT-htt-transfected cells, expression of ^{GFP}polyQ-htt caused a significant decrease in mIPSC amplitude (Figures 7D, 7F, and 7G; ^{GFP}WT-htt: 34 ± 5.0 pA, n = 6, ^{GFP}polyQ-htt: 13.7 ± 1.4 pA, n = 6, p < 0.05), which was also indicated by a leftward shift toward lower amplitudes in the cumulative distribution plot (Figure 7D). Although polyQ-htt caused a significant reduction in mIPSC amplitude (Figure 7H, 59.7% ± 4.1%, p < 0.05), it had little effect on mIPSC frequency (Figures 7E, 7F, and 7H). Expressing ^{GFP}polyQ-htt also resulted in a significant decrease in the area of GABA_AR clusters in neuronal dendrites compared with control ^{GFP}WT-htt-transfected cells (41.5% ± 11.5% of control, n = 5, p < 0.01, Figure 7I, 7J), but not the ratio of synaptic to nonsynaptic GABA_AR clusters at the cell surface (Figure S7F). These results clearly demonstrate that mutant polyQ-htt disrupts delivery of GABA_AR to synapses, leading to compromised inhibitory synaptic transmission.

DISCUSSION

We have analyzed the mechanisms that regulate the rapid transport of GABA_ARs to synapses. We demonstrate that delivery of GABA_ARs from internal compartments to surface and synaptic sites is dependent on a HAP1-KIF5 motor protein complex. Electrophysiological recordings in the present study

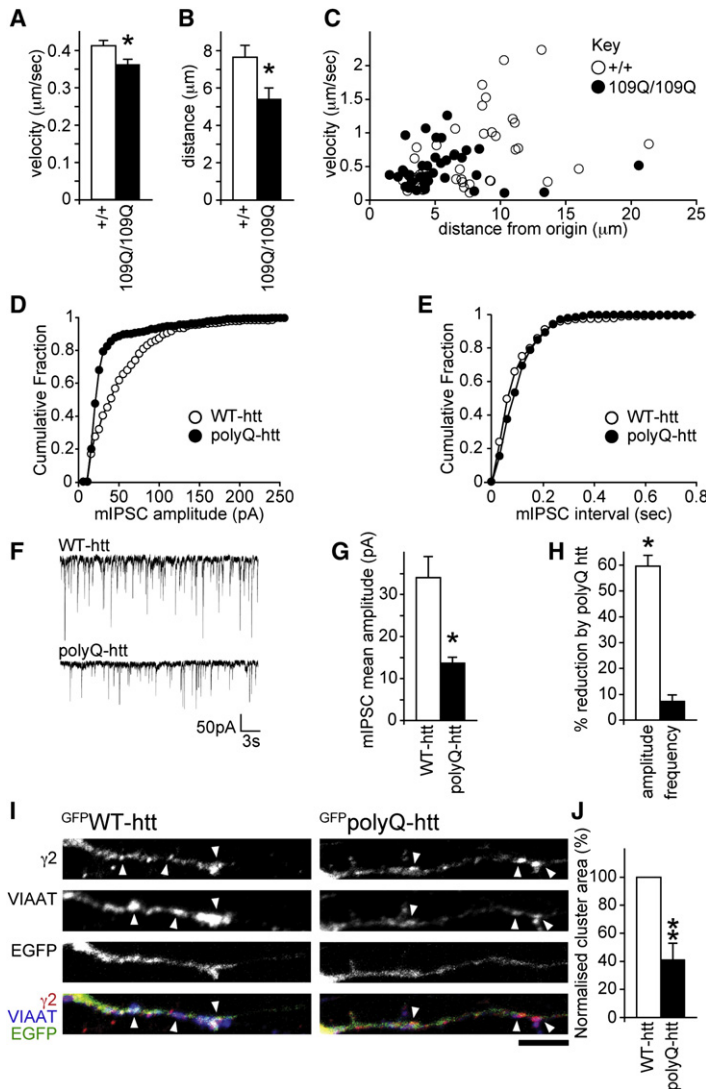


Figure 7. PolyQ-htt Disrupts GABA_AR Trafficking and Reduces Synaptic Inhibition

(A–C) WT (+/+) or 109Q/109Q neuronal cells expressing $\alpha 1$, $\beta 3$, and GFP $\gamma 2$ subunits were used to analyze the trafficking of GFP $\gamma 2$ vesicles in real time by video microscopy. (A) Average velocity \pm SEM ($\mu\text{m/s}$) of moving vesicles was reduced in 109Q/109Q cells compared with +/+ controls (2001 and 2082 measures respectively, three independent experiments).

(B) The mean total distance \pm SEM (μm) each vesicle has moved from its origin is longer in +/+ cells compared with 109Q/109Q cells (40 and 38 tracks respectively, three independent experiments) demonstrating a decreased processivity in mutant 109Q cells.

(C) The distance from origin versus the average velocity of each vesicle track was plotted. The main population of GFP $\gamma 2$ vesicles in 109Q/109Q cells move more slowly and for shorter distances compared with control WT (+/+) cells.

(D–H) Whole-cell recordings of mIPSCs from neurons transfected with either GFP $\gamma 2$ polyQ-htt or GFP $\gamma 2$ WT-htt control. Cumulative distribution plots show the mIPSC amplitude shifts to lower amplitudes in GFP $\gamma 2$ polyQ-htt transfected neurons, compared with GFP $\gamma 2$ WT-htt transfected neurons (D), while there is no change in mIPSC frequency (E). Representative traces (F) demonstrating reduction in mIPSC sizes in cells transfected with GFP $\gamma 2$ polyQ-htt, compared with GFP $\gamma 2$ WT-htt transfected cells. Summary bar graphs (G and H) show the average (mean \pm SEM) mIPSC amplitude in neurons transfected with GFP $\gamma 2$ WT-htt or GFP $\gamma 2$ polyQ-htt, and the percentage (mean \pm SEM) reduction in mIPSC amplitude and interval by polyQ-htt compared with WT-htt ($n = 6$; * $p < 0.05$).

(I and J) GABA_AR cluster analysis in neurons expressing GFP $\gamma 2$ WT-htt or GFP $\gamma 2$ polyQ-htt constructs reveals a reduction in synaptic $\gamma 2$ clusters (arrowheads) in GFP $\gamma 2$ polyQ-htt transfected neurons compared with GFP $\gamma 2$ WT-htt control (scale bar = 5 μm). Error bars, SEM; $n = 5$ experiments, 19–20 neurons; ** $p < 0.01$ (Student's t test).

provide evidence that KIF5-dependent trafficking of GABA_ARs to synapses is a critical regulator of rapid synaptic GABA_AR delivery and of the strength of the inhibitory synapses. This mechanism is likely to be a locus for regulation of trafficking of GABA_ARs during inhibitory synaptic plasticity and homeostasis.

In agreement with an important role for KIF5 and HAP1 in regulating GABA_AR transport, we find that GABA_ARs, KIF5 and HAP1 interact in vivo and that KIF5 is localized at inhibitory postsynaptic domains (Figure 2). Furthermore, using protein interaction mapping experiments, we reveal that KIF5 heavy chains interact directly with HAP1 via a C-terminal domain in KIF5 and the central HAP1-N-terminal homology domain rich in coiled coils (Figure 3). An earlier report demonstrated a direct interaction between a C-terminal region of HAP1 and the KLC (McGuire et al., 2006). However, we observed a much weaker direct interaction of the KLC with HAP1 compared with KIF5B and KIF5C in our pull-down assay, and we find the KLC binding domain of KIF5 is not necessary for the direct high-affinity interaction between KIF5 heavy chains and HAP1 (Figure 2). Thus, HAP1

acts as the adaptor protein directly linking GABA_AR transport vesicles to KIF5 heavy chains for their trafficking along microtubules. Further work is needed to determine if KLC plays an additional regulatory role in the GABA_AR-HAP1-KIF5 complex. There are a large number of KIF motors (Miki et al., 2001), and we cannot discount the possibility that other KIFs could interact with HAP1 and contribute to GABA_AR trafficking. However, we show here for at least one other KIF isoform (KIF17) that a direct interaction with HAP1 was not detected, and moreover that KIF17 activity does not contribute to inhibitory synapse function, supporting the specificity of the KIF5 interaction with HAP1 and its role in GABA_AR trafficking.

To test the functional significance of HAP1/KIF5-dependent GABA_AR trafficking in regulating surface and synaptic GABA_AR number, we examined the consequences for inhibitory synaptic currents of directly blocking KIF5 function or inhibiting the HAP1-KIF5 linkage to GABA_ARs. Acutely dialyzing KIF5 function blocking antibody via the electrophysiological recording pipette resulted in a rapid decrease in mIPSC amplitude, demonstrating a crucial role of KIF5 motor proteins in delivering GABA_ARs to synapses on rapid timescales (Figure 1). Transducing neurons with the same antibody also reduced GABA_AR cluster area, as determined by immunofluorescence and CLSM. Transfection of neurons with the HAP1 binding domain of KIF5 to compete with HAP1 for binding to KIF5, or using RNAi to knock down HAP1 and decrease the amount of HAP1-KIF5 complex present,

significantly decreased surface GABA_AR number, insertion of GABA_ARs into the membrane from the internal pool, GABA_AR cluster area, and the amplitude of mIPSCs (Figures 3–6). Expressing the KIF5 binding domain of HAP1 also significantly reduced the amplitude of mIPSCs. Moreover, knockdown of HAP1 also substantially reduced the number and run length of GABA_AR transport vesicles. Our observed 35%–45% reduction of mIPSC size presumably reflects an action on the actively trafficked pool of receptors, which is in agreement with the observed effects on receptor trafficking and receptor insertion into the membrane. In contrast, disrupting KIF5-dependent trafficking did not alter surface TrfR or NMDAR levels or the size of NMDAR responses, and blocking the function of the KIF17 motor for NMDARs did not effect GABAergic mIPSCs. Thus, the number of surface and synaptic GABA_ARs can be specifically controlled by the extent of HAP1-KIF5-dependent membrane insertion of GABA_ARs from the internal receptor pool to the postsynaptic membrane. In addition to being a potential locus for regulation of GABA_AR trafficking during inhibitory synaptic plasticity and homeostasis, HAP1/KIF5-dependent GABA_AR trafficking during the embryonic and early postnatal period, when GABA_ARs can be excitatory (Ben-Ari et al., 2007), may also be important for inhibitory synapse and circuit development.

Changes in the trafficking of GABA_ARs to and from the postsynaptic membrane are likely to underlie plasticity of GABAergic synapses in pathological conditions such as stroke and epilepsy, leading to alterations in inhibition and neuronal excitability (Mielke and Wang, 2005; Naylor et al., 2005). HAP1 interacts with huntingtin, the protein product mutated (by an expanded polyQ tract) in HD. HAP1-dependent motor protein trafficking of vesicles is modified by mutant polyQ-htt and may underlie cell death in HD (Gauthier et al., 2004). Our data suggest that HAP1-KIF5-dependent GABA_AR transport is disrupted by mutant polyQ-htt in HD. PolyQ-htt slowed the GABA_AR vesicle transport speed, resulting in a reduced delivery and number of GABA_ARs at inhibitory synapses, and a reduced inhibitory synaptic response (Figure 7). HAP1 interacts more tightly with polyQ-htt compared with WT huntingtin (Li et al., 1995). Wild-type huntingtin, via an interaction with HAP1, may be an integral component of the HAP1-KIF5 complex and traffic with GABA_AR vesicles. In HD pathology, polyQ-htt may remain associated with GABA_AR transport vesicles, but alter the function of the HAP1-KIF5 complex to disrupt the efficiency of GABA_AR vesicle trafficking. Alternatively, mutant polyQ-htt may disrupt the trafficking by sequestering HAP1 and KIF5 motors away from GABA_AR transport vesicles. Further work will be needed to determine which mechanism results in mutant polyQ-htt disrupting HAP1-KIF5 dependent GABA_AR trafficking.

Altered KIF5 motor-protein-dependent GABA_AR trafficking may directly contribute to reduced synaptic inhibition and altered information processing in HD. PolyQ-htt-dependent enhancement in NMDA receptor function and trafficking are proposed to exacerbate excitotoxicity in HD (Fan et al., 2007; Zeron et al., 2002). Furthermore, increased neurotransmission and neuronal excitability are also proposed to contribute to the neuronal degeneration caused by full-length polyQ-htt early in pathology (Romero et al., 2008) and early deficits in cortical inhibition have also been reported (Gu et al., 2005). Whether

polyQ-htt could also influence GABA_AR trafficking, synapse development, and inhibitory network function early during the development of GABAergic pathways is an interesting possibility and it is intriguing to note that in infants with early onset HD, the symptoms often include epileptic seizures (Harper, 2002). At later stages, disrupted GABA_AR trafficking to synapses and compromised inhibition caused by mutant htt is likely to also inhibit a homeostatic response to potentiated excitatory synaptic activity and neuronal excitability in HD, and thus significantly contribute to pathological “anti-homeostasis,” leading to further disruption of the excitatory/inhibitory balance and increased neuronal excitotoxicity. This raises the possibility of a new therapeutic target in HD: blocking recruitment of polyQ-htt to HAP1, so that disruption of KIF5-dependent trafficking of GABA_ARs to synapses is prevented.

EXPERIMENTAL PROCEDURES

Details regarding antibodies, immunofluorescence staining and analysis, molecular biology, and plasmid constructs are included in the [Supplemental Experimental Procedures](#).

Electron Microscopy

Adult Sprague-Dawley rats were anesthetized with pentobarbital (60 mg/kg) and intracardially perfused with 4% paraformaldehyde (PFA) and 0.1% glutaraldehyde in phosphate-buffered saline (PBS). After dissection, the cervical spinal cord and hippocampal tissue were kept overnight at 4°C in 4% PFA. Vibratome sections (100 μm) were cryoprotected for 3 hr in 20% glycerol and 20% sucrose at room temperature. They were then permeabilized by freezing-thawing, extensively rinsed in PBS, and immersed for 20 min in 50 mM ammonium chloride and for 30 min in PBS with 0.1% gelatin (PBSg). For immunogold detection of KIF5, vibratome sections were incubated for 12 hr (4°C) in the anti-KIF5 antibody and antibody binding sites detected using secondary nanogold-coupled antibody (1% in PBSg, Nanoprobe, Stony Brook, NY). Gold particles were intensified with HQ silver kit (Nanoprobe) and subsequently gold-toned (Gardioli et al., 1999). Immunoperoxidase methods (Colin et al., 1998) were used for the detection of GAD and KIF5C. For double detection of KIF5 and GAD (Figures 2e and 2f) the KIF5 detection procedure was performed first. After gold toning, the sections were subsequently kept overnight (4°C) in anti-GAD before immunoperoxidase detection. After dehydration and osmification, the sections were flat-embedded. Observations of ultrathin sections (pale yellow) were contrasted with uranyl acetate and Reynolds lead citrate (Poole, UK). Images were collected with a JEOL 100CXII electron microscope (Paris, France).

Immunoprecipitation Assays from Rat Brain Homogenates

Adult rat brains were homogenized on ice in 10 ml buffer (50 mM HEPES [pH 7.5], 0.5% Triton X-100, 150 mM NaCl, 1 mM EDTA, 1 mM PMSF in the presence of antipain, pepstatin, and leupeptin) then left to rotate at 4°C for 2 hr. Membranes were pelleted by ultracentrifugation at ~66,000 g for 40 min at 4°C. Protein content of the supernatant was assayed by Bio-Rad protein assay. Then 2–5 mg protein was transferred to a 1.5 ml microcentrifuge tube and made up to 500 μl with homogenization buffer. For coimmunoprecipitations 1–2 μg primary antibody was added in parallel to a suitable nonimmune IgG control antibody (Santa Cruz Biotechnology) of the same species. Samples were incubated overnight at 4°C with rotation. Complexes were precipitated with 15 μl of 50% protein A (for rabbit antibodies) or protein G (for goat antibodies) sepharose bead slurry (Generon) for 1 hr at 4°C. Beads were then washed three times by centrifugation and resuspension in 1 ml homogenization buffer. Samples were suspended in 3X protein sample buffer and analyzed by SDS-PAGE and western blotting.

Pull-Down Assays

Affinity purifications, using GST-fusion proteins purified from *E. coli*, were performed as described in a number of previous studies (Kittler et al., 2005,

2000a). For pull downs from rat brain, 50 μ g GST fusion protein immobilized on agarose beads was incubated in rat brain homogenate for 2 hr at 4°C, followed by five washes in homogenization buffer. Complexes were washed five times with pull-down buffer and then analyzed by SDS-PAGE and western blotting. For pull downs from transfected COS cells, transfected cells were harvested 24 hr posttransfection. Then 10 cm dishes of COS cells were solubilized in 0.5 ml pull-down buffer (50 mM HEPES [pH 7.5], 0.5% Triton, 150 mM NaCl, 1 mM EDTA, 1 mM PMSF in the presence of antipain, pepstatin, and leupeptin) for 45 min at 4°C. Detergent solubilized extracts were collected following centrifugation for 10 min at 17,900 g, 4°C, placed in a fresh 1.5 ml microcentrifuge tube, and incubated with 20 μ g of GST fusion protein for 2 hr. Complexes were washed five times with pull-down buffer and then analyzed by SDS-PAGE and western blotting with mouse anti-GFP (Roche). For pull downs with radiolabeled protein, KIF5A, KIF5B, KIF5C, and KLC1 were in vitro translated (IVT) from their appropriate pRK5 vectors using TNT SP6 Quick coupled Transcription/Translation system (Promega) and labeled with [³⁵S]-methionine (Perkin Elmer) following the manufacturer's instructions, with a 50 μ l final volume. Then 10–15 μ l IVT S³⁵ labeled protein was incubated for 2 hr with 10 μ g GST fusion protein immobilized on glutathione agarose beads in a final volume of 500 μ l, diluted in pull-down buffer. Complexes were washed three times in pull-down buffer and resolved by SDS-PAGE. Gels were dried and radioactivity detected using a storage phosphor screen.

Cell Culture, Transfection and Transduction

COS and HEK cells were maintained as described previously and transfected using electroporation (Kittler et al., 2000a, 2000b). The neuronal cells (109Q/109Q and +/-) derived from knockin mice (Trettel et al., 2000) were cultured in DMEM supplemented with 10% FBS, PenStrep, 40 μ g/ml G418, 1% glutamine and sodium pyruvate. Cortical, hippocampal, and striatal cultures were isolated from E18 or P0 Sprague-Dawley rats as described in a number of previous publications (Banker and Goslin, 1998; Chen et al., 2006; Kittler et al., 2004; Macaskill et al., 2009). Cultures for biotinylation experiments were transfected using Amaxa nucleofector technology using program O-003 and plated onto poly-L-lysine prepared 10 cm dishes. +/- and 109Q/109Q cultures for live video microscopy were transfected using Amaxa nucleofector technology using program T27 and plated onto coverslips for imaging. Striatal cultures for surface labeling and analysis of GABA_AR clusters were transfected by a calcium phosphate method as previously described (Kittler et al., 2006) at 7–10 days in vitro (DIV) and allowed to express for at least 3 days before fixation. Monoclonal antibodies (affinity purified SUK4, or 9E10 antibody as a control) were transduced across the plasma membrane of DIV 10–14 neurons using Chariot reagent (Active Motif) following the manufacturer's instructions with minor modifications (Coulpier et al., 2002; Kittler et al., 2006; Ma et al., 2006). In brief, per well of a 24 well plate, 2 μ l Chariot reagent was diluted in 50 μ l water before precomplexing with 20 μ g antibody in 50 μ l PBS for 30 min. The 100 μ l of complexed antibody/chariot was then overlaid onto the cultured neurons with 100 μ l fresh complete neuronal culture medium and left to incubate at 37°C for 1 hr. Another 400 μ l of fresh medium was then overlaid on the neurons and incubation was continued for 12 hr before cells were fixed and stained (see Supplemental Experimental Procedures).

Video Microscopy

All live imaging of transfected GABA_ARs was performed in imaging media (10 mM HEPES [pH 7.4], 125 mM NaCl, 5 mM KCl, 2 mM CaCl₂, 1 mM MgCl₂, 10 mM D-glucose, 285–300 mOsm) at 35°C–37°C under constant perfusion using an Ixon EM-CCD camera (Andor) on an upright Olympus BX51WI microscope. 109Q/109Q and +/- neuronal cell lines were transfected with either $\alpha\beta\gamma$ ^{GFP} or $\alpha\beta\gamma$ ^{dsRed} with GFP-KIF5B-HBD or pEGFP and movies were captured at 0.5 or 2 Hz. Movies of calcium phosphate transfected cultured cortical neurons were captured at 1 Hz. Illumination was provided by a high-intensity arc lamp with GFP visualized with an excitation filter of 470 nm (bandwidth 40 nm) and an emission filter of 525 nm (bandwidth 40 nm) and DsRed visualized with an excitation filter of 535 nm (bandwidth 40 nm) and an emission filter 620 nm (bandwidth 40 nm). Vesicle velocities were calculated from captured movies by analyses with either the "Track Points" macro of Metamorph (Universal Imaging) or ImageJ software using plugins available from the ImageJ website (<http://rsb.info.nih.gov/ij/plugins/>) as follows. To readily

identify vesicles over a noisy background in neurons, images were filtered using the spot enhancer filter from the SpotTracker plugin (D. Sage). Where coverslip drift was visible, images were corrected with the Stackreg plugin (P. Thevenaz). Individual moving vesicles were tracked manually using Mtrack J plugin (E. Meijering). Kymographs were made using the multiple kymograph function (J. Rietdorf). For mitochondrial velocity measurements, striatal cells were transfected with mtDsRed2 (Clontech). This construct contains DsRed fluorescent protein targeted to mitochondria via the targeting peptide of cytochrome-c oxidase. Cells were imaged under constant perfusion of imaging media at 36°C using a Zeiss Pascal upright confocal microscope and LSM software with an Achroplan 63 \times water-immersion lens with 0.95 numerical aperture. Images were acquired at 1 Hz. Excitation was via a HeNe laser at λ = 543 nm. Mitochondrial velocity was measured as for vesicles above.

Surface Biotinylation Assay

Nucleofected cultured cortical cultures were kept at 4°C and rinsed with PBS (all washing steps were performed in PBS supplemented with 1 mM CaCl₂ and 0.5 mM MgCl₂) before incubation with 0.5 mg/ml EZ-Link Sulfo-NHS-SS-Biotin (Pierce) for 12 min. The surface biotinylation reaction was quenched using three washes of 1 mg/ml BSA in Mg²⁺/Ca²⁺ supplemented PBS. Cells were washed and solubilized in 360 μ l RIPA buffer (50 mM Tris [pH 7.5], 1 mM EDTA, 2 mM EGTA, 150 mM NaCl, 1% NP40, 0.5% DOC, 0.1% SDS, 1 mM PMSF with antipain, pepstatin, and leupeptin) for 1 hr at 4°C. Cell membranes were pelleted at 14,000 rpm for 10 min at 4°C. Then 60 μ l (20%) was kept to analyze as an input. The remainder was incubated with 50 μ l UltraLink Neutra-vidin bead slurry (Pierce) for 2 hr at 4°C. Beads were washed twice with high-salt (0.5 M NaCl) RIPA buffer and once with normal (0.15 M NaCl) RIPA buffer. Complexes were separated by SDS-PAGE and analyzed by western blotting. GABA_AR β 3 subunit was detected with rabbit anti-GABA_AR- β 3 subunit as primary antibody and [125I]-labeled donkey anti-rabbit (Perkin Elmer) as secondary antibody. Radioactivity of western blots was detected using a storage phosphor screen.

For biotin endocytosis assays, nucleofected cortical cultures were surface biotinylated as above and following quenching, media was returned to the dishes and neurons were incubated at 37°C for 30 min to allow internalization. Cleavage of remaining surface biotin was carried out at 4°C by two 15 min incubations in cleavage solution (50 mM glutathione, 10 mM EDTA, 75 mM NaCl, 1% BSA [pH 7.8]). Cultures were solubilized and complexes precipitated as for surface biotinylations. Reinsertion biotinylation assays of cortical cultures were performed as described previously (Kittler et al., 2004). Briefly, cortical neurons were labeled with biotin and receptors were allowed to internalize for 30 min (the period for maximal receptor internalization [Kittler et al., 2004]), before cleavage with glutathione. Neurons were then incubated at 37°C for further time periods with glutathione in the external culture medium to cleave any internalized biotinylated receptors recycling to the cell surface. The loss of biotinylated internalized GABA_AR β 3 subunit after the second biotin cleavage provides a measure of receptor recycling (Ehlers, 2000). Internal β 3-subunit levels remaining were then compared with those at the start of the second incubation period with glutathione, designated as 100%.

Whole-Cell Recordings

Whole-cell recordings of mIPSCs from cultured neurons were performed using standard voltage-clamp techniques (Chen et al., 2006; Kittler et al., 2004). Electrodes were filled with the following internal solution: 100 mM CsCl, 30 mM N-methyl-D-glucamine, 10 mM HEPES, 1 mM MgCl₂, 1 mM EGTA, 5 mM QX314, 12 mM phosphocreatine, 5 mM MgATP, 1.5 mM Na₂GTP, 0.1 mM leupeptin [pH = 7.2–7.3], 265–270 mOsm/l. The neurons were recorded in tetrodotoxin (0.5 μ M) and held at –70 mV. Recordings of whole-cell ion channel currents used standard voltage-clamp techniques as described previously (Yuen et al., 2008, 2005). The internal solution contains the following: 180 mM N-methyl-D-glucamine, 40 mM HEPES, 4 mM MgCl₂, 0.5 mM BAPTA, 12 mM phosphocreatine, 3 mM Na₂ATP, 0.5 mM Na₂GTP, and 0.1 mM leupeptin [pH 7.2–7.3], 265–270 mOsm/l. The external solution consisted of the following: 127 mM NaCl, 20 mM CsCl, 10 mM HEPES, 1 mM CaCl₂, 5 mM BaCl₂, 12 mM glucose, 0.001 mM TTX, and 0.02 mM glycine (pH 7.3–7.4, 300–305 mOsm/l). GABA (100 μ M) or NMDA (100 μ M) was applied for 2 s every 30 s via a gravity-fed "sewer pipe" system using

capillaries (150 μ m inner diameter) positioned a few hundred micrometers from the neuron under study. The membrane holding potential was -40 mV and -70 mV for GABA and NMDA currents, respectively. Data were analyzed with Axograph (Axon Instruments, Union City, CA), Kaleidagraph (Albeck Software, Reading, PA) and Mini Analysis program (Synaptosoft, Leonia, NJ).

SUPPLEMENTAL INFORMATION

Supplemental Information includes seven figures, one table, two movies, and Supplemental Experimental Procedures, and can be found with this article online at doi:10.1016/j.neuron.2009.12.007.

ACKNOWLEDGMENTS

J.T.K. is supported by the U.K. Medical Research Council. We also acknowledge support from the European Commission Coordination Action ENINET (contract number LSHM-CT-2005-19063). We are very grateful to Marcie MacDonald and Elisa Fossale for generously providing the striatal wild-type and 109Q knockin cells and Anne Stephenson for providing the KIF5C-MD and -NMD constructs. We thank James Muir and David Attwell for comments on the manuscript.

Accepted: November 23, 2009

Published: January 13, 2010

REFERENCES

- Arancibia-Carcamo, I.L., and Kittler, J.T. (2009). Regulation of GABA(A) receptor membrane trafficking and synaptic localization. *Pharmacol. Ther.* **123**, 17–31.
- Banker, G., and Goslin, K. (1998). *Culturing Nerve Cells*, Second Edition (Cambridge: MA: The MIT Press).
- Ben-Ari, Y., Gaiarsa, J.L., Tyzio, R., and Khazipov, R. (2007). GABA: a pioneer transmitter that excites immature neurons and generates primitive oscillations. *Physiol. Rev.* **87**, 1215–1284.
- Bi, G.Q., Morris, R.L., Liao, G., Alderton, J.M., Scholey, J.M., and Steinhardt, R.A. (1997). Kinesin- and myosin-driven steps of vesicle recruitment for Ca²⁺-regulated exocytosis. *J. Cell Biol.* **138**, 999–1008.
- Chen, G., Kittler, J.T., Moss, S.J., and Yan, Z. (2006). Dopamine D3 receptors regulate GABAA receptor function through a phospho-dependent endocytosis mechanism in nucleus accumbens. *J. Neurosci.* **26**, 2513–2521.
- Colin, I., Rostaing, P., Augustin, A., and Triller, A. (1998). Localization of components of glycinergic synapses during rat spinal cord development. *J. Comp. Neurol.* **398**, 359–372.
- Coulpier, M., Anders, J., and Ibanez, C.F. (2002). Coordinated activation of autophosphorylation sites in the RET receptor tyrosine kinase: importance of tyrosine 1062 for GDNF mediated neuronal differentiation and survival. *J. Biol. Chem.* **277**, 1991–1999.
- Dumoulin, A., Rostaing, P., Bedet, C., Levi, S., Isambert, M.F., Henry, J.P., Triller, A., and Gasnier, B. (1999). Presence of the vesicular inhibitory amino acid transporter in GABAergic and glycinergic synaptic terminal boutons. *J. Cell Sci.* **112**, 811–823.
- Ehlers, M.D. (2000). Reinsertion or degradation of AMPA receptors determined by activity-dependent endocytic sorting. *Neuron* **28**, 511–525.
- Engelender, S., Sharp, A.H., Colomer, V., Tokito, M.K., Lanahan, A., Worley, P., Holzbaur, E.L., and Ross, C.A. (1997). Huntingtin-associated protein 1 (HAP1) interacts with the p150Glued subunit of dynactin. *Hum. Mol. Genet.* **6**, 2205–2212.
- Fan, M.M., and Raymond, L.A. (2007). N-methyl-D-aspartate (NMDA) receptor function and excitotoxicity in Huntington's disease. *Prog. Neurobiol.* **81**, 272–293.
- Fan, M.M., Fernandes, H.B., Zhang, L.Y., Hayden, M.R., and Raymond, L.A. (2007). Altered NMDA receptor trafficking in a yeast artificial chromosome transgenic mouse model of Huntington's disease. *J. Neurosci.* **27**, 3768–3779.
- Gardioli, A., Racca, C., and Triller, A. (1999). Dendritic and postsynaptic protein synthetic machinery. *J. Neurosci.* **19**, 168–179.
- Gauthier, L.R., Charrin, B.C., Borrell-Pages, M., Dompierre, J.P., Rangone, H., Cordelieres, F.P., De Mey, J., MacDonald, M.E., Lessmann, V., Humbert, S., and Saudou, F. (2004). Huntingtin controls neurotrophic support and survival of neurons by enhancing BDNF vesicular transport along microtubules. *Cell* **118**, 127–138.
- Gu, X., Li, C., Wei, W., Lo, V., Gong, S., Li, S.H., Iwasato, T., Itoharu, S., Li, X.J., Mody, I., et al. (2005). Pathological cell-cell interactions elicited by a neuropathogenic form of mutant Huntingtin contribute to cortical pathogenesis in HD mice. *Neuron* **46**, 433–444.
- Guillaud, L., Setou, M., and Hirokawa, N. (2003). KIF17 dynamics and regulation of NR2B trafficking in hippocampal neurons. *J. Neurosci.* **23**, 131–140.
- Gunawardena, S., Her, L.S., Brusch, R.G., Laymon, R.A., Niesman, I.R., Gordesky-Gold, B., Sintasath, L., Bonini, N.M., and Goldstein, L.S. (2003). Disruption of axonal transport by loss of huntingtin or expression of pathogenic polyQ proteins in *Drosophila*. *Neuron* **40**, 25–40.
- Harper, P.S. (2002). *Huntington's Disease*, Volume 45 (London: Oxford University Press).
- Hirokawa, N., and Takemura, R. (2005). Molecular motors and mechanisms of directional transport in neurons. *Nat. Rev.* **6**, 201–214.
- Ingold, A.L., Cohn, S.A., and Scholey, J.M. (1988). Inhibition of kinesin-driven microtubule motility by monoclonal antibodies to kinesin heavy chains. *J. Cell Biol.* **107**, 2657–2667.
- Jacob, T.C., Moss, S.J., and Jurd, R. (2008). GABA(A) receptor trafficking and its role in the dynamic modulation of neuronal inhibition. *Nat. Rev.* **9**, 331–343.
- Jaulin, F., Xue, X., Rodriguez-Boulant, E., and Kreitzer, G. (2007). Polarization-selective transport to the apical membrane by KIF5B in MDCK cells. *Dev. Cell* **13**, 511–522.
- Kittler, J.T., Delmas, P., Jovanovic, J.N., Brown, D.A., Smart, T.G., and Moss, S.J. (2000a). Constitutive endocytosis of GABAA receptors by an association with the adaptin AP2 complex modulates inhibitory synaptic currents in hippocampal neurons. *J. Neurosci.* **20**, 7972–7977.
- Kittler, J.T., Wang, J., Connolly, C.N., Vicini, S., Smart, T.G., and Moss, S.J. (2000b). Analysis of GABAA receptor assembly in mammalian cell lines and hippocampal neurons using gamma 2 subunit green fluorescent protein chimeras. *Mol. Cell. Neurosci.* **16**, 440–452.
- Kittler, J.T., Thomas, P., Tretter, V., Bogdanov, Y.D., Haucke, V., Smart, T.G., and Moss, S.J. (2004). Huntingtin-associated protein 1 regulates inhibitory synaptic transmission by modulating gamma-aminobutyric acid type A receptor membrane trafficking. *Proc. Natl. Acad. Sci. USA* **101**, 12736–12741.
- Kittler, J.T., Chen, G., Honing, S., Bogdanov, Y., McAinsh, K., Arancibia-Carcamo, I.L., Jovanovic, J.N., Pangalos, M.N., Haucke, V., Yan, Z., and Moss, S.J. (2005). Phospho-dependent binding of the clathrin AP2 adaptor complex to GABAA receptors regulates the efficacy of inhibitory synaptic transmission. *Proc. Natl. Acad. Sci. USA* **102**, 14871–14876.
- Kittler, J.T., Hanley, J.G., and Issac, J.T.R. (2006). Transfecting and transducing neurons with synthetic nucleic acids and biologically active macromolecules. In *The Dynamic Synapse: Molecular Methods in Ionotropic Receptor Biology*, J.T. Kittler and S.J. Moss, eds. (CRC Press).
- Lane, J.D., and Allan, V.J. (1999). Microtubule-based endoplasmic reticulum motility in *Xenopus laevis*: activation of membrane-associated kinesin during development. *Mol. Biol. Cell* **10**, 1909–1922.
- Li, X.J., and Li, S.H. (2005). HAP1 and intracellular trafficking. *Trends Pharmacol. Sci.* **26**, 1–3.
- Li, X.J., Li, S.H., Sharp, A.H., Nucifora, F.C., Jr., Schilling, G., Lanahan, A., Worley, P., Snyder, S.H., and Ross, C.A. (1995). A huntingtin-associated protein enriched in brain with implications for pathology. *Nature* **378**, 398–402.
- Li, S.H., Gutekunst, C.A., Hersch, S.M., and Li, X.J. (1998). Interaction of huntingtin-associated protein with dynactin P150Glued. *J. Neurosci.* **18**, 1261–1269.
- Ma, Y., Li, J., Chiu, I., Wang, Y., Sloane, J.A., Lu, J., Kosaras, B., Sidman, R.L., Volpe, J.J., and Vartanian, T. (2006). Toll-like receptor 8 functions as a negative

- regulator of neurite outgrowth and inducer of neuronal apoptosis. *J. Cell Biol.* 175, 209–215.
- Macaskill, A.F., Rinholm, J.E., Twelvetrees, A.E., Arancibia-Carcamo, I.L., Muir, J., Fransson, A., Aspenstrom, P., Attwell, D., and Kittler, J.T. (2009). Miro1 is a calcium sensor for glutamate receptor-dependent localization of mitochondria at synapses. *Neuron* 67, 541–555.
- McGuire, J.R., Rong, J., Li, S.H., and Li, X.J. (2006). Interaction of huntingtin-associated protein-1 with kinesin light chain: Implications in intracellular trafficking in neurons. *J Biol Chem.* 281, 3552–3559.
- Mielke, J.G., and Wang, Y.T. (2005). Insulin exerts neuroprotection by counteracting the decrease in cell-surface GABA receptors following oxygen-glucose deprivation in cultured cortical neurons. *J. Neurochem.* 92, 103–113.
- Miki, H., Setou, M., Kaneshiro, K., and Hirokawa, N. (2001). All kinesin superfamily protein, KIF, genes in mouse and human. *Proc. Natl. Acad. Sci. USA* 98, 7004–7011.
- Morris, M.C., Depollier, J., Mery, J., Heitz, F., and Divita, G. (2001). A peptide carrier for the delivery of biologically active proteins into mammalian cells. *Nat. Biotechnol.* 19, 1173–1176.
- Naylor, D.E., Liu, H., and Wasterlain, C.G. (2005). Trafficking of GABA(A) receptors, loss of inhibition, and a mechanism for pharmacoresistance in status epilepticus. *J. Neurosci.* 25, 7724–7733.
- Oikkonen, V.M., and Ikonen, E. (2006). When intracellular logistics fails—genetic defects in membrane trafficking. *J. Cell Sci.* 119, 5031–5045.
- Romero, E., Cha, G.H., Verstreken, P., Ly, C.V., Hughes, R.E., Bellen, H.J., and Botas, J. (2008). Suppression of neurodegeneration and increased neurotransmission caused by expanded full-length huntingtin accumulating in the cytoplasm. *Neuron* 57, 27–40.
- Setou, M., Nakagawa, T., Seog, D.H., and Hirokawa, N. (2000). Kinesin superfamily motor protein KIF17 and mLin-10 in NMDA receptor-containing vesicle transport. *Science* 288, 1796–1802.
- Smith, R., Brundin, P., and Li, J.Y. (2005). Synaptic dysfunction in Huntington's disease: a new perspective. *Cell. Mol. Life Sci.* 62, 1901–1912.
- Szebenyi, G., Morfini, G.A., Babcock, A., Gould, M., Selkoe, K., Stenoien, D.L., Young, M., Faber, P.W., MacDonald, M.E., McPhaul, M.J., and Brady, S.T. (2003). Neuropathogenic forms of huntingtin and androgen receptor inhibit fast axonal transport. *Neuron* 40, 41–52.
- Trettel, F., Rigamonti, D., Hilditch-Maguire, P., Wheeler, V.C., Sharp, A.H., Persichetti, F., Cattaneo, E., and MacDonald, M.E. (2000). Dominant phenotypes produced by the HD mutation in STHdh(Q111) striatal cells. *Hum. Mol. Genet.* 9, 2799–2809.
- Yuen, E.Y., Jiang, Q., Chen, P., Gu, Z., Feng, J., and Yan, Z. (2005). Serotonin 5-HT1A receptors regulate NMDA receptor channels through a microtubule-dependent mechanism. *J. Neurosci.* 25, 5488–5501.
- Yuen, E.Y., Jiang, Q., Chen, P., Feng, J., and Yan, Z. (2008). Activation of 5-HT2A/C receptors counteracts 5-HT1A regulation of n-methyl-D-aspartate receptor channels in pyramidal neurons of prefrontal cortex. *J. Biol. Chem.* 283, 17194–17204.
- Zeron, M.M., Hansson, O., Chen, N., Wellington, C.L., Leavitt, B.R., Brundin, P., Hayden, M.R., and Raymond, L.A. (2002). Increased sensitivity to N-methyl-D-aspartate receptor-mediated excitotoxicity in a mouse model of Huntington's disease. *Neuron* 33, 849–860.